ROBUST STRUCTURED GROUP LOCAL SPARSE TRACKER USING DEEP FEATURES

Mohammadreza Javanmardi, Amir Hossein Farzaneh, Xiaojun Qi

Department of Computer Science, Utah State University, Logan, UT 84322-4205, USA

ABSTRACT

Sparse representation has recently been successfully applied in visual tracking. It utilizes a set of templates to represent target candidates and find the best one with the minimum reconstruction error as the tracking result. In this paper, we propose a robust deep features-based structured group local sparse tracker (DF-SGLST), which exploits the deep features of local patches inside target candidates and represents them by a set of templates in the particle filter framework. Unlike the conventional local sparse trackers, the proposed optimization model in DF-SGLST employs a group-sparsity regularization term to seamlessly adopt local and spatial information of the target candidates and attain the spatial layout structure among them. To solve the optimization model, we propose an efficient and fast numerical algorithm that consists of two subproblems with the closed-form solutions. Different evaluations in terms of success and precision on the benchmarks of challenging image sequences (e.g., OTB50 and OTB100) demonstrate the superior performance of the proposed tracker against several state-of-the-art trackers.

Index Terms— Visual Tracking, Sparse Representation, Convolutional Neural Network, Convex Optimization

1. INTRODUCTION

Visual tracking aims to estimate states of a moving object in a dynamic frame sequence. It has been considered as one of the most paramount and challenging topics in computer vision with a large variety of applications in human motion analysis, surveillance, smart vehicles transportation, navigation, etc. Although numerous tracking methods [1, 2, 3, 4, 5, 6] have been introduced in recent years, developing a robust algorithm that is able to handle different challenges such as occlusion, illumination variations, deformation, fast motion, moving camera, background clutter, and low resolution still remains unsolved.

During the past few years, various sparse representation based trackers (sparse trackers) have been proposed. They aim to find the best target region with the minimum reconstruction error among a set of target candidates [7, 8, 5, 9, 10]. Generally, sparse representation is a dictionary learning process, which sparsely represents the input data by a linear combination of basis elements. It has played a dominant role in various computer vision applications including face recognition [11], image denoising and restoration [12], image segmentation [13, 14], image pansharpening [15], etc. Sparse trackers usually utilize a convex optimization model to represent the appearance of target candidates in the particle filter framework. Based on the spatial information of target regions integrated in the optimization model, sparse trackers are classified into three categories: global, local, and global-local trackers.

In global sparse trackers, the holistic region in each target candidate is represented by the template set. As one of the pioneer global sparse trackers, Mei et al. [7] represent the global information of target candidates by a set of templates using ℓ_1 minimization. Bao et al. [16] present an accelerated proximal gradient descent method to efficiently solve ℓ_1 minimization. In order to attain the relationship among target candidates, Zhang et al. [17] propose to learn the global information of all target candidates in a joint sparse appearance model. Later, Hong et al. [18] cast tracking as a multi-task multi-view sparse learning problem in terms of the least square (LS). Mei et al. [8] further use the least absolute deviation (LAD) in the optimization model to handle the data contaminated by outliers and noise. In general, these global sparse trackers achieve good performance. However, they model each target region as a holistic entity and may fail when targets undergo heavy occlusions in a frame sequence.

Unlike global sparse trackers, local sparse trackers represent local patches inside target candidates by local patches inside templates. Liu et al. [19] introduce a local sparse tracker by adopting the histogram of sparse coefficients and a sparse constrained regularized mean-shift algorithm. This tracker is based on a static local sparse dictionary and therefore fails in the cases when similar objects co-exist in the scene. To address the shortcomings of the static local sparse dictionary, Jia et al. [9] exploit both partial and spatial information of target candidates and represent them in a dynamic local sparse dictionary. Jia et al. [20] further propose to extract coarse and fine local patches inside each target candidate to improve the tracking performance. Despite favorable performance, these local sparse trackers [9, 20] fail to consider the spatial layout structure among local patches inside a target candidate. As a result, the sparse vectors of local patches inside a target candidate exhibit a random and dissimilar pattern (or structure) on the non-zero elements.

Global-local sparse trackers are hybrid trackers and con-

sider both global and local information of all target candidates in their optimization models to improve the tracking performance. Zhang et al. [5] represent local patches inside all target candidates along with the global information using $\ell_{1,2}$ norm regularization on the representation matrix. They assume that the same local patches of all target candidates are similar. However, this assumption does not hold true in practice due to outliers and occlusions. To address this shortcoming, Zhang et al. [10] design an optimal target region searching method to take into account issues related to outliers and occlusions. These hybrid sparse trackers achieve improved tracking performance. However, considering the relationship of all target candidates degrades the performance when drifting occurs. Furthermore, using $\ell_{1,2}$ norm regularization in the optimization model to integrate local and global information of target candidates lessens the tracking accuracy in the cases of heavy occlusions.

In this paper, we propose a robust deep features-based structured group local sparse tracker (DF-SGLST), which exploits the convolutional neural network (CNN) deep features of the local patches inside a target candidate and represent them in a novel convex optimization model. The proposed optimization model in DF-SGLST employs a group-sparsity regularization term to adopt local and spatial information of the target candidates and attain the spatial layout structure among them. The major contributions of the proposed work are summarized as follows:

- Proposing a deep features-based structured local sparse tracker, which employs CNN deep features of the local patches within a target candidate and attains the spatial structure among the features of local patches inside a target candidate.
- Developing a convex optimization model, which introduces a group-sparsity regularization term to encourage the tracker to sparsely select the corresponding local patches of the same subset of templates to represent the CNN deep features of local patches of each target candidate.
- Designing a fast and parallel numerical algorithm based on the alternating direction method of multiplier (ADMM), which consists of two subproblems with closed-form solutions to efficiently and quickly solve the optimization model.

The remainder of this paper is organized as follows: Section 2 reviews some representative conventional and most up-to-date trackers. Section 3 introduces the notations used in the paper. Section 4 presents the DF-SGLST together with its new convex optimization model solved by the proposed ADMM-based numerical solution, and explains the deep feature extraction and the template updates strategies. Section 5 demonstrates the experimental results on OTB50 and OTB100 challenging tracking benchmarks, compares the DF-SGLST with several state-of-the-art trackers, and discusses the results and future work. Section 6 draws the conclusions.

2. OTHER REPRESENTATIVE STATE-OF-THE-ART TRACKERS

In addition to the aforementioned sparse trackers, other visual tracking methods have been proposed during the past couple of years. In this section, we review some of the most representative discriminative, generative, correlation filter-based, and CNN-based tracking methods, which are related to our proposed tracker.

Discriminative tracking methods cast the tracking problem as binary classification and formulate a decision boundary to distinguish the target from backgrounds. As one of the pioneer work, Avidan [21] introduces the ensemble tracker to combine a set of weak classifiers into a strong one to label the candidate as either a target or background. To alleviate the drifting problem in tracking applications, Grabner et al. [22] propose an online semi-supervised boosting method, which formulates the update process in a semi-supervised manner as combined decision of a given prior and an online classifier. Bebenko et al. [23] present an online multiple instance learning framework to update the appearance model for object tracking using a large number of positive and negative image patches.

Unlike discriminative tracking methods, generative methods adopt a model to represent the target and formulate the tracking problem as a model-based searching procedure to find the most similar region to the target. For instance, Black et al. [24] design the eigenspace model to represent the target and employ a coarse-to-fine matching strategy to track the target in a video sequence. Adam et al. [25] propose a Frag tracker to handle partial occlusions and pose changes in the image sequences. The Frag tracker represents a template object using multiple arbitrary image fragments (patches) and uses the integral histogram to combine the vote maps of the multiple patches to track a target. Ross et al. [26] propose to incrementally learn a low-dimensional subspace representation of the target and adapt the learned representation to changes in pose, view angle, and illumination.

Correlation filter-based tracking methods [27, 28, 29, 30] have recently gained significant attention due to their fast learning and detection. They regress all the circular shift of the input features to a target Gaussian function in the Fourier domain. As one of the superior work, Henriques et al. [28] propose a method by using the fast Fourier transform of circulant shifts of a target candidate with several types of kernels including the popular Gaussian and polynomial kernels. Ma et al. [29] encode both semantics and spatial details of the target objects to improve the tracking performance by exploiting features extracted from different convolutional layers of CNN and adaptively learning correlation filters at each layer. To handle large scale variations, Danelljan et al. [30]

estimate the target scale in a tracking-by-detection framework by learning discriminative correlation filters based on a scale pyramid representation.

Recently, convolutional neural networks (CNNs) have been applied to visual tracking with tremendous improvement [31, 32, 28, 33, 34, 35, 10]. As one of the pioneer work, Wang and Yeung [31] propose a multi-layer denoising autoencoder network to learn generic image features that are more robust against variations for visual tracking. Later, Wang et al. [36] use auxiliary video sequences to learn hierarchical features, which are robust to both complicated motion transformations and appearance changes of target objects, via a two-layer CNN. They then integrate the feature learning algorithm into three tracking methods to achieve significant improvement. Similarly, CNN hierarchical features are also integrated in some correlation filter-based trackers and sparse trackers [28, 33, 10] to achieve better tracking performance than using other low-level hand-engineered features. Some deep learning-based tracking methods [37, 38] have also demonstrated impressive performance by using external videos to pretrain a network before online tracking .

3. NOTATIONS

Throughout this paper, matrices, vectors, and scalers are denoted by boldface uppercase, boldface lowercase, and italic lowercase letters, respectively. For a given matrix $\mathbf{X}$, $\mathbf{X}_{i,j}$ denotes the element at the i^{th} row and j^{th} column, $\|\mathbf{X}\|_{\mathrm{F}}$ indicates the Frobenious norm, $\|\mathbf{X}\|_{p,q}$ is the ℓ_p norm of ℓ_q norm of the rows in $\mathbf{X}$, and $\mathbf{X}(:)$ is the vectorized form of $\mathbf{X}$. For a given column vector $\mathbf{x}$, $\mathrm{diag}(\mathbf{x})$ and $\mathbf{x}_i$ denote a diagonal matrix formed by the elements of $\mathbf{x}$ and the i^{th} element of $\mathbf{x}$, respectively. Symbol $\mathrm{tr}(\cdot)$ stands for the trace operator, $\mathbf{X} \otimes \mathbf{Y}$ is the Kronecker product on two matrices $\mathbf{X}$ and $\mathbf{Y}$ of arbitrary sizes, $\mathbf{1}_l$ is a column vector of all ones with the dimension of l, and $\mathbf{I}_k$ denotes a $k \times k$ identity matrix.

4. PROPOSED METHOD

This section presents the proposed deep features-based structured group local sparse tracker (DF-SGLST). Specifically, subsection 4.1 formulates a local sparse appearance model in DF-SGLST, whose convex optimization model addresses the drawbacks of conventional local sparse trackers [9, 20]. Subsection 4.2 describes an efficient numerical algorithm in detail, which solves the convex optimization problem presented in subsection 4.1. Subsection 4.3 presents the local deep feature extraction. Subsection 4.4 describes the template update strategy.

4.1. Deep Features-Based Structured Group Local Sparse Tracker (DF-SGLST)

The proposed DF-SGLST utilizes both local and spatial information of target candidates in the particle filter framework and employs a new optimization model to achieve robust tracking performance. The new optimization model attains the spatial layout structure among different local patches inside a target candidate to achieve a consistent and similar pattern (or structure) on the non-zero elements of the sparse vector, which effectively addresses the drawback of conventional local sparse trackers.

Conventional local sparse trackers [9, 20] individually represent local patches without taking into consideration of their spatial layout structure. For instance, local patches in [9] are separately represented by solving the Lasso problem. As a result, local patches inside a target candidate may be sparsely represented by the corresponding local patches inside *different* dictionary templates. Figure 1(a) clearly illustrates that two local patches of the j^{th} target candidate, shown in the red and blue bounding boxes, may be represented by the corresponding local patches in different dictionary templates.

In this paper, we propose a novel DF-SGLST that adopts both local and spatial information of target candidates to achieve robust tracking performance. The proposed tracker employs a new optimization model to solve the aforementioned issues associated with conventional local sparse trackers [9, 20]. Specifically, DF-SGLST formulates an optimization problem, which seamlessly imposes a structure on the sparse vectors of different local patches inside each target candidate and attains the spatial layout structure among the local patches. Roughly speaking, the proposed optimization model ensures that local patches of a target candidate are represented by their corresponding patches in the *same* dictionary templates. For example, if the r^{th} local patch of the j^{th} target candidate is best represented by the r^{th} local patch of the q^{th} template, the s^{th} local patch of the j^{th} target candidate is also be best represented by the s^{th} local patch of the q^{th} template. Figure 1(b) demonstrates this improvement, where both local patches of the j^{th} target candidate, shown in the red and blue bounding boxes, are represented by their corresponding patches in the *same* dictionary templates (e.g., the first and the tenth templates). To solve the proposed model, we develop an efficient numerical algorithm consisting of two subproblems with closed-form solutions by adopting the alternating direction method of multiplier (ADMM).

We first use k target templates, select l overlapping local patches inside each template, and extract a d-dimensional feature vector for each patch to construct the dictionary $\mathbf{D}$. Such a representation generates the local feature dictionary matrix $\mathbf{D} = [\mathbf{D}_1, \ldots, \mathbf{D}_k] \in \mathbb{R}^{d \times (lk)}$, where $\mathbf{D}_i \in \mathbb{R}^{d \times l}$. We then construct a matrix $\mathbf{X} = [\mathbf{X}_1, \ldots, \mathbf{X}_n] \in \mathbb{R}^{d \times (ln)}$, which contains the local features of all the target candidates, where n is the number of particles (target candidates). Next, we define

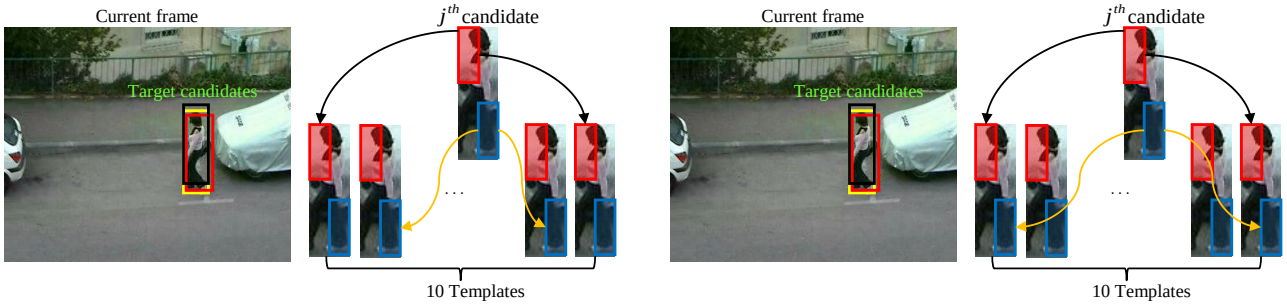

Fig. 1: Illustration of the sparse representation of two sample local patches of the j^{th} target candidate in: (a) Conventional local sparse trackers [9, 20]. One local patch of the j^{th} target candidate, shown in the red bounding box, is represented by its corresponding patch in the first and the tenth templates, while another local patch of this candidate, shown in the blue bounding box, is represented by its corresponding patch in two different templates (e.g., the second and the ninth templates). (b) The proposed DF-SGLST. Both local patches of the j^{th} target candidate, shown in red and blue bounding boxes, are represented by their corresponding patches in the same templates (e.g., the first and the tenth templates).

the matrix coefficients $\mathbf{C}$ corresponding to the j^{th} target candidate as $\mathbf{C} \triangleq \begin{bmatrix}\mathbf{C}_1 & \cdots & \mathbf{C}_k\end{bmatrix}^\top \in \mathbb{R}^{(lk)\times l}$, where $\{\mathbf{C}_q\}_{q=1}^k$ is a $l \times l$ matrix indicating the group representation of the l local features of the j^{th} target candidate using the l local features of the q^{th} template. Finally, we formulate the following convex model:

$$\underset{\mathbf{C}\in\mathbb{R}^{(lk)\times l}}{\text{minimize}} \quad \|\mathbf{X}_j - \mathbf{D}\mathbf{C}\|_{\mathrm{F}}^2 + \lambda \left\| \begin{bmatrix}\mathbf{C}_1(:) \dots \mathbf{C}_k(:)\end{bmatrix}^\top \right\|_{1,\infty} \tag{1a}$$

$$\text{subject to} \quad \mathbf{C} \geq 0, \tag{1b}$$

$$\mathbf{1}_{lk}^\top \mathbf{C} = \mathbf{1}_l^\top, \tag{1c}$$

where the first term is the total cost of representing feature matrix $\mathbf{X}_j$ using the dictionary matrix $\mathbf{D}$ and the second term is a group-sparsity regularization term, which penalizes the objective function in proportion to the number of selected templates (dictionary words). Moreover, the group-sparsity regularization term imposes all the local features to jointly select similar few templates by simultaneously establishing the $\|\cdot\|_{1,\infty}$ minimization on matrix $\mathbf{C}$. The regularization parameter $\lambda > 0$ balances the trade-off between the first and the second terms. The constraint (1c) ensures that each local feature vector in $\mathbf{X}_j$ is expressed by at least one selected local feature vector of the dictionary $\mathbf{D}$ and the sum of a linear combination of coefficients is constrained.

For each target candidate, we find the sparse matrix $\mathbf{C}$ using the numerical algorithm presented in subsection 4.2. We then perform an averaging process together with an alignment pooling strategy [9] to find a representative vector. Finally, we add all the elements in this representative vector as the likelihood value, where high value indicates high possibility to contain an object. As a result, we select the candidate with the highest likelihood value as the tracking result for each frame. It should be mentioned that we also update the templates throughout the sequence using the same strategy proposed in [9] to handle the appearance variations of the target region.

4.2. Numerical Algorithm

This section presents a numerical algorithm based on the alternating direction method of multipliers (ADMM) [39] to efficiently solve the proposed model (1). The idea of ADMM is to utilize auxiliary variables to convert a complex convex problem to smaller sub-problems, where each sub-problem is efficiently solvable via an explicit formula. The ADMM iteratively solves the sub-problems until it converges. To do so, we first define vector $\mathbf{m} \in \mathbb{R}^k$ such that $\mathbf{m}_i = \arg\max |\mathbf{C}_i(:)|$ and rewrite (1) as:

$$\underset{\substack{\mathbf{C}\in\mathbb{R}^{(lk)\times l}\\ \mathbf{m}\in\mathbb{R}^k}}{\text{minimize}} \quad \|\mathbf{X}_j - \mathbf{D}\mathbf{C}\|_{\mathrm{F}}^2 + \lambda \mathbf{1}_k^\top \mathbf{m} \tag{2a}$$

$$\text{subject to} \quad \mathbf{C} \geq 0, \tag{2b}$$

$$\mathbf{1}_{(lk)}^\top \mathbf{C} = \mathbf{1}_l^\top, \tag{2c}$$

$$\mathbf{m} \otimes \mathbf{1}_l \mathbf{1}_l^\top \geq \mathbf{C}. \tag{2d}$$

The inequality constraint (2d) is imposed in the above reformulation to ensure the equivalence between (1) and (2). It can be transformed into an equality one by introducing a non-negative slack matrix $\mathbf{U} \in \mathbb{R}^{(lk)\times l}$, which compensates the difference between $\mathbf{m} \otimes \mathbf{1}_l \mathbf{1}_l^\top$ and $\mathbf{C}$. Therefore, (2) is rewrit-

ten as:

$$\begin{aligned}\underset{\substack{\mathbf{C},\mathbf{U}\in\mathbb{R}^{(lk)\times l}\\ \mathbf{m}\in\mathbb{R}^k}}{\text{minimize}} \quad & \|\mathbf{X}_j-\mathbf{D}\mathbf{C}\|_{\mathrm{F}}^2+\lambda\mathbf{1}_k^\top\mathbf{m} && \text{(3a)}\\ \text{subject to} \quad & \mathbf{C}\geq 0, && \text{(3b)}\\ & \mathbf{1}_{(lk)}^\top\mathbf{C}=\mathbf{1}_l^\top, && \text{(3c)}\\ & \mathbf{m}\otimes\mathbf{1}_l\mathbf{1}_l^\top=\mathbf{C}+\mathbf{U}, && \text{(3d)}\\ & \mathbf{U}\geq 0. && \text{(3e)}\end{aligned}$$

The equality constraint (3d) implies that the columns of $\mathbf{C}+\mathbf{U}$ are regulated to be identical. Hence, it can be simply replaced by a linear constraint independent of $\mathbf{m}$ as presented in (4d). Moreover, $\mathbf{1}_k^\top\mathbf{m}$ can be equivalently written as $\frac{1}{l^2}\mathbf{1}_{(lk)}^\top(\mathbf{C}+\mathbf{U})\mathbf{1}_l$ using (3d). Therefore, we rewrite (3) independent of $\mathbf{m}$ as:

$$\begin{aligned}\underset{\mathbf{C},\mathbf{U}\in\mathbb{R}^{(lk)\times l}}{\text{minimize}} \quad & \|\mathbf{X}_j-\mathbf{D}\mathbf{C}\|_{\mathrm{F}}^2+\frac{\lambda}{l^2}\mathbf{1}_{(lk)}^\top(\mathbf{C}+\mathbf{U})\mathbf{1}_l && \text{(4a)}\\ \text{subject to} \quad & \mathbf{C}\geq 0, && \text{(4b)}\\ & \mathbf{1}_{(lk)}^\top\mathbf{C}=\mathbf{1}_l^\top, && \text{(4c)}\\ & \mathbf{E}(\mathbf{C}+\mathbf{U})=\frac{\mathbf{I}_k\otimes\mathbf{1}_l\mathbf{1}_l^\top}{l}(\mathbf{C}+\mathbf{U}), && \text{(4d)}\\ & \mathbf{U}\geq 0, && \text{(4e)}\end{aligned}$$

where matrix $\mathbf{E}$ serves as the right circular shift operator on the rows of $\mathbf{C}+\mathbf{U}$. To construct the ADMM formulation, whose sub-problems possess closed-form solutions, we define auxiliary variables $\hat{\mathbf{C}},\hat{\mathbf{U}}\in\mathbb{R}^{(lk)\times l}$ and reformulate (4) as:

$$\begin{aligned}\underset{\mathbf{C},\hat{\mathbf{C}},\mathbf{U},\hat{\mathbf{U}}\in\mathbb{R}^{(lk)\times l}}{\text{minimize}} \quad & \|\mathbf{X}_j-\mathbf{D}\mathbf{C}\|_{\mathrm{F}}^2+\frac{\lambda}{l^2}\mathbf{1}_{(lk)}^\top(\mathbf{C}+\mathbf{U})\mathbf{1}_l\\ & +\frac{\mu_1}{2}\left\|\mathbf{C}-\hat{\mathbf{C}}\right\|_{\mathrm{F}}^2+\frac{\mu_2}{2}\left\|\mathbf{U}-\hat{\mathbf{U}}\right\|_{\mathrm{F}}^2 && \text{(5a)}\\ \text{subject to} \quad & \hat{\mathbf{C}}\geq 0, && \text{(5b)}\\ & \mathbf{1}_{(lk)}^\top\hat{\mathbf{C}}=\mathbf{1}_l^\top && \text{(5c)}\\ & \mathbf{E}(\mathbf{C}+\mathbf{U})=\frac{\mathbf{I}_k\otimes\mathbf{1}_l\mathbf{1}_l^\top}{l}(\mathbf{C}+\mathbf{U}), && \text{(5d)}\\ & \hat{\mathbf{U}}\geq 0, && \text{(5e)}\\ & \mathbf{C}=\hat{\mathbf{C}},\ \ \mathbf{U}=\hat{\mathbf{U}}. && \text{(5f)}\end{aligned}$$

where $\mu_1,\mu_2>0$ are the augmented Lagrangian parameters. Without loss of generality, we assume $\mu=\mu_1=\mu_2$ [39]. The last two terms in the objective function (5a) are vanished for any feasible solutions, which implies (4) and (5) are equivalent. We further form the augmented Lagrangian function to solve (5) as follows:

$$\begin{aligned}\mathcal{L}_\mu(\mathbf{C},\mathbf{U},\hat{\mathbf{C}},\hat{\mathbf{U}},\mathbf{\Lambda}_1,\mathbf{\Lambda}_2)=&\ \|\mathbf{X}_j-\mathbf{D}\mathbf{C}\|_{\mathrm{F}}^2+\frac{\lambda}{l^2}\mathbf{1}_{(lk)}^\top(\mathbf{C}+\mathbf{U})\mathbf{1}_l\\ &+\frac{\mu}{2}\left\|\mathbf{C}-\hat{\mathbf{C}}+\frac{\mathbf{\Lambda}_1}{\mu}\right\|_{\mathrm{F}}^2+\frac{\mu}{2}\left\|\mathbf{U}-\hat{\mathbf{U}}+\frac{\mathbf{\Lambda}_2}{\mu}\right\|_{\mathrm{F}}^2\end{aligned} \tag{6}$$

where $\mathbf{\Lambda}_1,\mathbf{\Lambda}_2\in\mathbb{R}^{(lk)\times l}$ are the Lagrangian multipliers corresponding to the equations in (5f). Given initialization for $\hat{\mathbf{C}}$, $\hat{\mathbf{U}}$, $\mathbf{\Lambda}_1$, and $\mathbf{\Lambda}_2$ at time $t=0$ (e.g., $\hat{\mathbf{C}}^0,\hat{\mathbf{U}}^0,\mathbf{\Lambda}_1^0,\mathbf{\Lambda}_2^0$), (6) is solved through the ADMM iterations described below:

$$\begin{aligned}(\mathbf{C}^{t+1},\mathbf{U}^{t+1}):=\ & \underset{\mathbf{C},\mathbf{U}\in\mathbb{R}^{(lk)\times l}}{\arg\min} \quad \mathcal{L}_\mu(\mathbf{C},\mathbf{U},\hat{\mathbf{C}}^t,\hat{\mathbf{U}}^t,\mathbf{\Lambda}_1^t,\mathbf{\Lambda}_2^t)\\ & \text{subject to} \quad \text{(5d)}\end{aligned} \tag{7}$$

$$\begin{aligned}(\hat{\mathbf{C}}^{t+1},\hat{\mathbf{U}}^{t+1}):=&\underset{\mathbf{C},\mathbf{U}\in\mathbb{R}^{(lk)\times l}}{\arg\min}\ \mathcal{L}_\mu(\mathbf{C}^{t+1},\mathbf{U}^{t+1},\hat{\mathbf{C}},\hat{\mathbf{U}},\mathbf{\Lambda}_1^t,\mathbf{\Lambda}_2^t)\\ &\text{subject to} \quad \text{(5b), (5c), (5e).}\end{aligned} \tag{8}$$

$$\begin{aligned}\mathbf{\Lambda}_1^{t+1}&=\mathbf{\Lambda}_1^t+\mu(\mathbf{C}^{t+1}-\hat{\mathbf{C}}^{t+1})\\ \mathbf{\Lambda}_2^{t+1}&=\mathbf{\Lambda}_2^t+\mu(\mathbf{U}^{t+1}-\hat{\mathbf{U}}^{t+1})\end{aligned} \tag{9}$$

By considering the quadratic and linear terms of $\mathbf{C}$ and $\mathbf{U}$ in (6), we first define $\{\mathbf{z}_i\}_{i=1}^{lk}$, where $\mathbf{z}_i\in\mathbb{R}^{2l}$ is obtained by stacking the i^{th} rows of $\mathbf{C}$ and $\mathbf{U}$. We then divide (7) into lk equality constrained quadratic programs as follows:

$$\begin{aligned}\underset{\mathbf{z}_i\in\mathbb{R}^{2l}}{\text{minimize}} \quad & \frac{1}{2}\mathbf{z}_i^\top\mathbf{Q}\mathbf{z}_i+\mathbf{z}_i^\top\mathbf{q}_i && \text{(10a)}\\ \text{subject to} \quad & \mathbf{A}\mathbf{z}_i=\mathbf{0} && \text{(10b)}\end{aligned}$$

where $\mathbf{Q}\in\mathbb{R}^{l\times l}$ is a block diagonal positive semi-definite matrix and $\mathbf{A}$ is a sparse matrix constructed based on the constraint (5d). Each of the above quadratic programs has its analytical solution by writing the KKT conditions.

Similarly, we split (8) into two separate sub-problems with closed-form solutions over $\hat{\mathbf{C}}$ and $\hat{\mathbf{U}}$ as follows:

$$\begin{aligned}\underset{\mathbf{z}_i\in\mathbb{R}^{2l}}{\text{minimize}} \quad & \left\|\hat{\mathbf{C}}-(\mathbf{C}+\frac{\mathbf{\Lambda}_1}{\mu})\right\|_{\mathrm{F}}^2 && \text{(11a)}\\ \text{subject to} \quad & \hat{\mathbf{C}}\geq 0, && \text{(11b)}\\ & \mathbf{1}_{(lk)}^\top\hat{\mathbf{C}}=\mathbf{1}_l^\top && \text{(11c)}\end{aligned}$$

$$\begin{aligned}\underset{\mathbf{z}_i\in\mathbb{R}^{2l}}{\text{minimize}} \quad & \left\|\hat{\mathbf{U}}-(\mathbf{U}+\frac{\mathbf{\Lambda}_2}{\mu})\right\|_{\mathrm{F}}^2 && \text{(12a)}\\ \text{subject to} \quad & \hat{\mathbf{U}}\geq 0 && \text{(12b)}\end{aligned}$$

where the sub-problem (11) consists of l independent Euclidean norm projections onto the probability simplex constraints and the sub-problem (12) consists of l independent Euclidean norm projections onto the non-negative orthant. Both sub-problems (11) and (12) have analytical solutions. Finally, we solve the two sub-problems over $\mathbf{\Lambda}_1$ and $\mathbf{\Lambda}_2$ in (9) by performing l parallel updates over their respective columns. All these iterative updates can be quickly performed due to the closed-form solutions.

4.3. Local Deep Feature Extraction

In the proposed DF-SGLST tracker, we automatically extract learned local deep features to represent each target region. To this end, we set the size of each target candidate to 64×64 pixels to contain sufficient object-level information with decent resolution. Each target candidate is passed to the pre-trained VGG19 [40] network to automatically extract their representative features. This network has been proven to achieve better performance in tracking than other CNNs such as AlexNet since its strengthened semantic with deeper architecture is more insensitive to significant appearance change. The default input for VGG network is $224\times224\times3$. Therefore, each target candidate is resized to this default input size before forward propagation. We utilize the output of the *Conv5-4* layer as the feature map of the target candidate since the fifth layer is proven to be effective in discriminating the targets even with dramatic background changes [29]. The dimensionality of this feature map is $14 \times 14 \times 512$. We further upsample this feature map to the size of $28 \times 28 \times 512$ using the same bilinear interpolation technique introduced in [29] to alleviate the issues that spatial resolution is gradually reduced with the increase of the depth of convolutional layers. To extract the local deep features, we employ the concept of shared features [41] to divide the upsampled feature map into $l = 9$ overlapping $14 \times 14 \times 512$ features maps with the stride of 7. The feature map of each of 9 overlapping patches is vectorized as a feature vector with the size of 1×100352. Finally, we apply principal component analysis (PCA) on the feature vector of each patch to attain the top 1120 principal components for each local feature vector (e.g., $d = 1120$) to speed up the process to find the best target candidate by the proposed optimization model.

4.4. Template Update

We adopt the same strategy as used in [9] to update templates. We generate a cumulative probability sequence and a random number according to uniform distribution on the unit interval $[0, 1]$. We then choose the template to be replaced based on the section that the random number lies in. This ensures that the old templates are slowly updated and the new ones are quickly updated. As a result, the drifting issues are alleviated.

We replace the selected template by using the information of the tracking result in the current frame. To do so, we represent the tracking result by a dictionary in a Lasso problem. This dictionary contains trivial templates (identity matrix) [7] and PCA basis vectors, which are calculated from the templates $\mathbf{D}$. We numerically solve the Lasso problem using the accelerated proximal gradient (APG) method. To further improve the computational time, we consider the structure of the identity matrix in our Lasso numerical solver to quickly perform the matrix multiplications and find the descend direction faster in each iteration.

5. EXPERIMENTAL RESULTS

In this section, we evaluate the performance of the proposed DF-SGLST and its two variants (i.e. SGLST_Color and SGLST_HOG) on the object tracking benchmark (OTB), which contains fully annotated videos with substantial variations. We evaluate these three trackers on both OTB50 [42] and OTB100 [43] benchmarks for fair comparison since not all the trackers provide the results on both benchmarks.

The two variants are similar to the proposed tracker except that SGLST_Color uses gray-level intensity features and SGLST_HOG uses histogram of oriented gradients (HOG) features to represent each local patch. We implement these two variants since both gray-level intensity and HOG features have shown promising tracking results in different trackers [9, 27, 8, 10]. To extract intensity features, we resize each target region to 32×32 pixels and extract $l = 9$ overlapping local patches of 16×16 pixels inside the target region using the stride of 8 pixels. As a result, we use $d = 256$ dimensional gray-level intensity features to represent local patches. To extract HOG features, we resize the target candidates to 64×64 pixels to contain sufficient edge-level information with decent resolution. We then exploit $d = 196$ dimensional HOG features [44] for $l = 9$ overlapping local patches of 32×32 inside the target region using the stride of 16 pixels. As a result, we use $d = 196$ dimensional HOG features to capture relatively high-resolution edge information to represent local patches.

For all the experiments, we set $\lambda = 0.1$, $\mu = \mu_1 = \mu_2 = 0.1$, the number of particles $n = 400$, and the number of templates $k = 10$. We initially set the variances of affine parameters for particle filter resampling as $(8, 8, 0.01, 0.001, 0.005, 0.0001)$ and adaptively update the resampling variances based on the tracking results. We use the maximum of the initial variance and the variance of the affine parameters of the most recent five tracking results to update the standard deviation of the affine parameters. We implement the proposed DF-SGLST in MATLAB with the MatConvNet toolbox [45] on a machine with a 3.60 GHz CPU, 32 GB RAM, and a 1080Ti 11 GB Nvidia GPU. The GPU is utilized for CNN forward propagation to extract deep features of 9 local patches for each target candidate.

5.1. Evaluation Metrics

We utilize two metrics, namely, bounding box overlap ratio and center location error [42, 43], to evaluate the performance of the proposed tracker and its two variants against other trackers. The overlap ratio between the tracked bounding box r_t and the ground truth bounding box r_g is defined as $S = \frac{|r_t \cap r_g|}{|r_t \cup r_g|}$, where $|\cdot|$ is the number of pixels in the bounding box, $\cap$ represents the intersection of the two bounding boxes, and $\cup$ represents the union of the two bounding boxes. The center location error is defined as the Euclidean distance between the center of the tracked bounding box r_t and the

ground truth bounding box r_g. We then plot the success plots based on the bounding box overlap ratio and plot the precision plots based on the center location error. Specifically, the success plots show the percentage of successful frames at the overlap ratio thresholds ranging from 0 to 1, where the successful frames are the ones who have overlap ratios larger than a given threshold. To rank the trackers using the success plots, we calculate the area under curve (AUC) score for each compared tracker on all image sequences. The tracker with the highest AUC score achieves the best overall performance and the tracker with the lowest AUC score achieves the worst overall performance in terms of the bounding box overlap ratio. The precision plots show the percentage of successful frames at the center location error thresholds ranging from 0 to 50 pixels. The successful frames are the ones who have the center location error less than a given threshold. To rank the trackers using the precision plots, we calculate the precision score at the threshold of 20 pixels [42, 43] for each compared tracker on all image sequences. The tracker with the highest precision score achieves the best overall performance and the tracker with the lowest precision score achieves the worst overall performance in terms of the center location error.

5.2. Experimental Results on OTB50

We conduct the experiments on OTB50 [42] to evaluate the overall performance of the proposed DF-SGLST and its two variants (i.e., SGLST_Color and SGLST_HOG) under different challenges. This benchmark consists of 50 annotated sequences, where 49 sequences has one annotated target and one sequence (*jogging*) has two annotated targets. Each sequence is also labeled with attributes specifying the presence of different challenges including illumination variation (IV), scale variation (SV), occlusion (OCC), deformation (DEF), motion blur (MB), fast motion (FM), in-plane rotation (IPR), out-of-plane rotation (OPR), out-of-view (OV), background clutter (BC), and low resolution (LR). The sequences are categorized based on the attributes and 11 challenge subsets are generated. These subsets are utilized to evaluate the performance of trackers in different challenge categories.

We compare DF-SGLST with its two variants (SGLST_Color and SGLST_HOG), 29 baseline trackers in [42], and 17 recent trackers including MTMVTLS [18], MTMVTLAD [8], MSLA [20] (the recent version of ASLA [9]), SST [5], SMTMVT [46], CNT [34], two variants of TGPR (i.e., TGPR_Color and TGPR_HOG) [47], DSST [30], PCOM [48], KCF [28], MEEM[49], SAMF [50], SRDCF [51], STAPLE [52], and two variants of RSST (i.e., RSST_HOG and RSST_Deep) [10]. Following the protocol proposed in [42], we use the same parameters on all the sequences to obtain the one-pass evaluation (OPE) results, which are conventionally used to evaluate trackers by initializing them using the ground truth location in the first frame. We present the overall OPE success and precision plots in Figure 2. We only include top 20 of the 49 compared trackers in each plot to avoid clutter and increase the readability. The value within the parenthesis alongside each legend of the success plots is the AUC score for the corresponding tracker. Similarly, the value within the parenthesis alongside each legend of the precision plots is the precision score for the corresponding tracker.

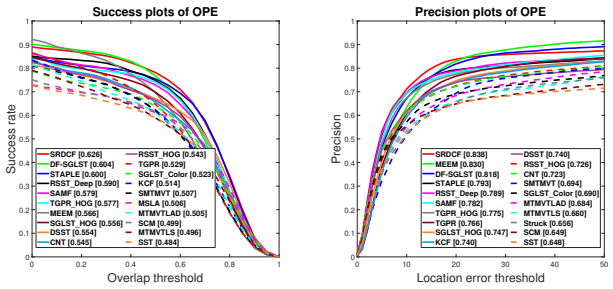

(a) Success plot of OPE (b) Precision plot of OPE

Fig. 2: The overall OPE plots for the 50 frame sequences in OTB50. (a) Overall OPE success plots; (b) Overall OPE precision plots.

It is clear from Figure 2 that incorporating deep features improves the tracking performance as the proposed DF-SGLST achieves better AUC and precision scores than its two variants, i.e., SGLST_HOG and SGLST_Color. The similar improvement trends are also observed in [10], where RSST_Deep achieves better performance than RSST_HOG. Among the 29 baseline trackers employed in [42], SCM [53] and Struck [54] achieve the most favorable performance. DF-SGLST significantly improves both baseline trackers. Specifically, it outperforms SCM and Struck by 21.04% and 24.73% in terms of the AUC scores, respectively. It outperforms SCM and Struck by 26.04% and 24.70% in terms of the precision

Score	L1APG	ASLA	MTT	MTMVTLAD	MSLA	SST	RSST			SGLST		
							Color	HOG	Deep	Color	HOG	Deep
AUC	0.380	0.434	0.376	0.505	0.506	0.484	0.520	0.543	0.590	0.523	0.556	**0.604**
Precision	0.485	0.532	0.479	0.684	0.631	0.648	0.691	0.726	0.789	0.690	0.747	**0.818**

Table 1: Summary of the tracking performance of the proposed tracker, its two variants, and nine representative sparse trackers on OTB50. Bold numbers indicate the highest AUC and precision scores (i.e., the best tracking performance). Note that the proposed tracker DF-SGLST is listed in the last column as SGLST_Deep.

scores, respectively. When comparing with the 17 additional recent trackers, DF-SGLST achieves higher AUC scores than 16 of these trackers and a comparable score as SRDCF (the best tracker in comparison). Specifically, it improves the AUC scores of MTMVTLAD, MSLA, KCF, CNT, DSST, MEEM, TGPR_HOG, SAMF, RSST_Deep, and STAPLE by 19.60%, 19.37%, 17.51%, 10.83%, 9.03%, 6.71%, 4.68%, 4.32%, 2.37%, and 0.67%, respectively. SRDCF shows slightly better performance than DF-SGLST (0.626 AUC score for SRDCF vs. 0.604 AUC score for DF-SGLST). DF-SGLST also achieves higher precision scores than 15 out of 17 additional recent trackers. Specifically, it outperforms MTMVTLAD, SMTMVT, CNT, DSST, KCF, TGPR_HOG, SAMF, RSST_Deep, and STAPLE by 19.59%, 17.87%, 13.14%, 10.54%, 10.54%, 5.55%, 4.60%, 3.68%, and 3.15%, respectively. It attains a comparable precision score as MEEM and SRDCF. All three trackers yields the precision scores above 0.81.

To demonstrate the effectiveness of the proposed optimization model, we compare the proposed tracker and its two variants (i.e., DF-SGLST, SGLST_HOG, and SGLST_Color) with representative traditional and recent sparse trackers in terms of the two evaluation metrics in Table 1. It is clear that DF-SGLST achieves the highest overall AUC and precision scores among all the compared sparse trackers. It improves RSST_Deep, one of the most recent sparse trackers that incorporates the deep features, by 2.37% in the AUC score and 3.68% in the precision score. Its two variants (SGLST_HOG, and SGLST_Color) also outperforms RSST's counterparts (RSST_HOG, and RSST_Color) in terms of two evaluation metrics except that SGLST_Color achieves the similar precision score as RSST_Color (0.690 vs. 0.691). In addition, SGLST_Color achieves higher AUC and precision scores than other sparse trackers that utilize intensity features such as L1APG [16], ASLA [9], MTT [55], MSLA [20], and SST [5]. SGLST_HOG also achieves higher AUC and precision scores than the sparse trackers that utilize HOG features such as MTMVTLAD [8] and RSST_HOG [10]. It is worthy of mentioning that SGLST attains significant improvements over conventional local sparse trackers (ASLA and MSLA) by preserving the spatial layout structures among different local patch features inside a target candidate. The robust tracking performance of the SGLST demonstrate the effectiveness of the proposed optimization model that employs a group-sparsity regularization term to adopt local and spatial information of the target candidates and attain the spatial layout structure among them.

In addition to sparse trackers, the proposed DF-SGLST achieves a better or comparable AUC score (0.604) than some correlation filter (CF) based trackers including KCF (0.514) [28], DSST (0.556) [30], LCT (0.612) [56], HDT (0.603) [33], CF2 (0.605) [29], and ACFN (0.607) [57]. It also achieves a better or comparable precision score (0.818) than the following CF-based trackers: KCF (0.740), DSST (0.740), LCT (0.848), HDT (0.889), CF2 (0.891), and ACFN (0.860).

Comparing with deep learning-based trackers, the proposed DF-SGLST outperforms or achieves a comparable AUC score than CNT (0.545) [34], GOTURN (0.444) [58], CNN-SVM (0.597) [59], FCNT (0.599) [32], DLSSVM (0.589) [35], and SiamFC (0.608) [60]. Moreover, it outperforms or achieves comparable precision score than CNT (0.723), GOTURN (0.620), CNN-SVM (0.852), FCNT (0.856), DLSSVM (0.829), and SiamFC (0.815).

We further evaluate the performance of DF-SGLST in terms of AUC and precision scores on each of 11 challenge subsets in OTB50. Figure 3 presents the success and precision plots for 11 challenge subsets of the top 20 trackers. Interested readers may refer to [42] for the results of the other trackers. The value within the parenthesis on the title line of each plot is the number of video sequences in the specific subset. The value within the parenthesis alongside each legend of the success plot is the AUC score for the corresponding tracker and the value within the parenthesis alongside each legend of the precision plots is the precision score for the corresponding tracker. It is clear from Figure 3 that DF-SGLST achieves better performance than its two variants, SGLST_HOG and SGLST_Color, due to the use of CNN deep features. In terms of the AUC scores in success plots, DF-SGLST ranks as one of the top three trackers for 5 challenge subsets including BC, IV, LR, OPR, and SV. It ranks the fourth for 2 subsets with DEF and OCC challenges and the fifth for the IPR challenge subset. In addition, it achieves the sixth rank for MB and FM challenge subsets. In terms of the precision scores in precision plots, DF-SGLST ranks as the first for 2 subsets with LR and SV challenges, the third for 3 subsets with BC, IV, and OPR challenges, the fifth for 4 subsets with DEF, OCC, MB, and FM challenges, and the sixth for the IPR challenge subset. DF-SGLST ranks the 11th for the OV challenge subset in terms of both evaluation measures.

5.3. Experimental Results on OTB100

We conduct the experiments on OTB100 [43] to evaluate the overall performance of the proposed DF-SGLST and its two variants under different challenges. This benchmark extends OTB50 [42] by adding 50 additional annotated sequences. Each sequence is labeled with attributes specifying the presence of different challenges. The two sequences, *jogging* and *Skating*, have two annotated targets. The rest of 98 sequences have one annotated target.

We evaluate the proposed DF-SGLST and its two variants (SGLST_HOG and SGLST_Color) against 29 baseline trackers in [43], and 15 recent trackers including DSST, PCOM, KCF, TGPR_HOG, MEEM, SAMF, SRDCF, LCT, STAPLE, CF2, CNN-SVM, DLSSVM, HDT, and two variants of RSST (i.e., RSST_HOG and RSST_Deep). Some trackers used in the experiments of OTB50 are excluded from this experiment since they do not publish their results on OTB100. Similar to

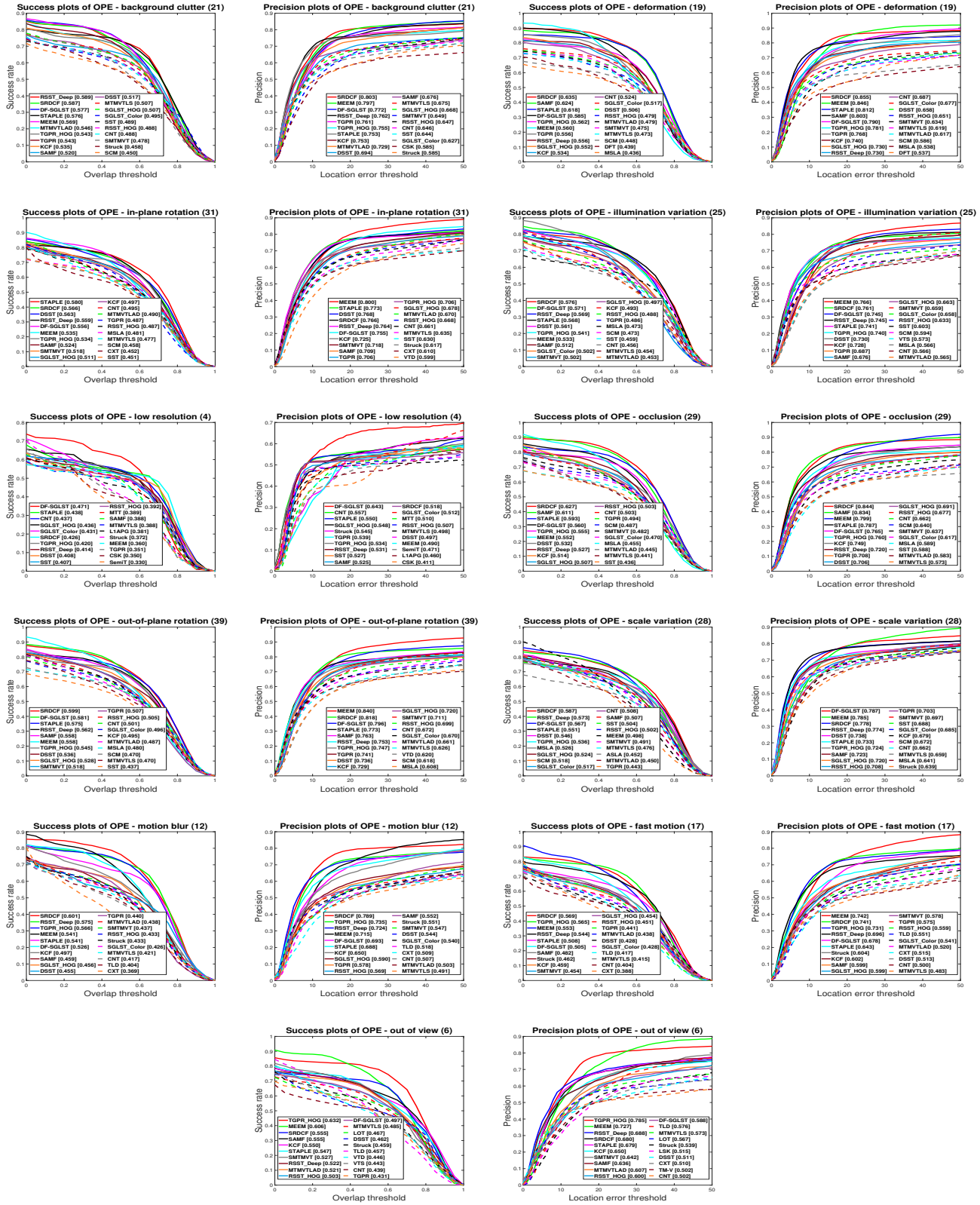

Fig. 3: The OPE success plots and precision plots for each of 11 challenge subsets in OTB50.

the experiments on OTB50, we follow the protocol proposed in [42, 43] and use the same parameters on all the sequences to obtain the OPE results. We present the overall OPE success and precision plots of the top 20 trackers out of 47 compared trackers in Figure 4.

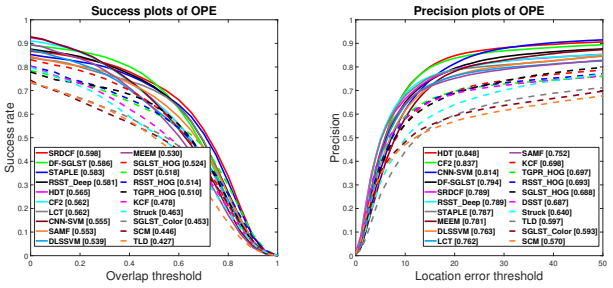

(a) Success plot of OPE (b) Precision plot of OPE

Fig. 4: The overall OPE plots for the 100 frame sequences in OTB100. (a) Overall OPE success plots; (b) Overall OPE precision plot.

It is clear from Figure 4 that the proposed DF-SGLST achieves higher AUC and precision scores than its two variants for 100 sequences in OTB100 due to its utility of local deep features. It also achieves higher AUC and precision scores than RSST_Deep due to its novel optimization model. Similar to the tracking results obtained on OTB50, SCM and Struck are the top two trackers among the 29 baseline trackers on OTB100. DF-SGLST improves the AUC scores of SCM and Struck by 31.39% and 26.57% and the precision scores of SCM and Struck by 39.30% and 24.06%, respectively. Compared to the 15 recent trackers, DF-SGLST achieves comparable AUC scores as SRDCF (0.586 vs. 0.598) and improves the AUC scores of the remaining 14 trackers. Specifically, it improves the AUC scores of the top 13 trackers, namely, KCF, TGPR_HOG, RSST_HOG, DSST, MEEM, DLSSVM, SAMF, CNN-SVM, LCT, CF2, HDT, RSST_Deep, and STAPLE by 22.59%, 14.90%, 14.01%, 13.13%, 10.57%, 8.72%, 5.97%, 5.59%, 4.27%, 4.27%, 3.72%, ,0.87%, and 0.52%, respectively. It also significantly improves the precision scores of six of these 15 trackers including SST, TGPR_HOG, KCF, SAMF, LCT, and DLSSVM by 15.57%, 13.92%, 13.75%, 5.59%, 4.20%, and 4.06%, respectively. In addition, it achieves a little bit improvement over four trackers including MEEM, STAPLE, RSST_Deep, and SRDCF. It is inferior to three trackers such as HDT, CF2, and CNN-SVM by a small margin.

The proposed DF-SGLST significantly outperforms conventional sparse trackers such as L1APG [16], LRST [17], ASLA [9], and MTT [55] and improves both AUC and precision scores of RSST_Deep [10], one of the most recent sparse trackers, by 0.87% and 0.64%, respectively. DF-SGLST with the achieved AUC score of 0.586 outperforms some CF-based trackers such as KCF (0.478), DSST (0.518), LCT (0.562), CF2 (0.562), and HDT (0.565) and some deep learning-based trackers such as GOTURN (0.427), CNN-SVM (0.555), and DLSSVM (0.539). These OTB100 tracking results follow the similar trends in OTB50 tracking results and demonstrate the effectiveness of the proposed optimization model and the integration of local deep features.

Similar to the experiments on OTB50, we further evaluate the performance of DF-SGLST in terms of AUC and precision scores on 11 challenge subsets in OTB100. Figure 5 shows the success and precision plots of the top 20 trackers for 11 challenge subsets using the same labeling as Figure 3. It is clear that DF-SGLST achieves significantly better performance than its two variants (SGLST_HOG and SGLST_Color) due to its integration of local deep features. In terms of the AUC scores, DF-SGLST ranks the best for two subsets with LR and OPR challenges, the second for two subsets with IV and OV challenges, the third for three subsets with BC, SV, and MB challenges, the fourth for the OCC subset, and the top eight trackers for three subsets with DEF, IPR, and FM challenges. In terms of the precision scores, DF-SGLST ranks as one of the top three trackers for five subsets with BC, IV, LR, OPR, and SV challenges, the fifth for four subsets with DEF, OCC, MB, and OV challenges, and the top eight trackers for two subsets with FM and IPR challenges.

5.4. Discussions

The proposed DF-SGLST has demonstrated superior tracking performance in terms of overall success and precision plots in comparison to representative conventional and recent sparse trackers [16, 20, 8, 5, 10]. It outperforms one of the most recent and powerful sparse trackers, RSST_Deep [10], in both OTB50 and OTB100. Specifically, it attains better performance than RSST_Deep when the target undergoes various challenges such as deformation, illumination variation, low resolution, occlusion, and out of plane rotations. However, similar to the other sparse trackers, DF-SGLST is less effective in handling targets with fast motion and motion blur, mainly due to the inefficiency of its particle filter resampling process to handle the fast motions of targets between consecutive frames.

The proposed DF-SGLST has also demonstrated superior tracking performance in comparison to some state-of-the-art CF trackers [30, 29, 33]. However, sparse trackers are more computational expensive than CF trackers since they have to solve an optimization model in each frame to find the target among a number of candidates. On the contrary, CF trackers use the fast Fourier transform to efficiently distinguish the target from backgrounds.

Furthermore, sparse trackers can barely recover successfully when drifts occur mainly due to the following two reasons: 1) The particle filter resampling is limited around the location of tracked target in the previous frame. 2) The tem-

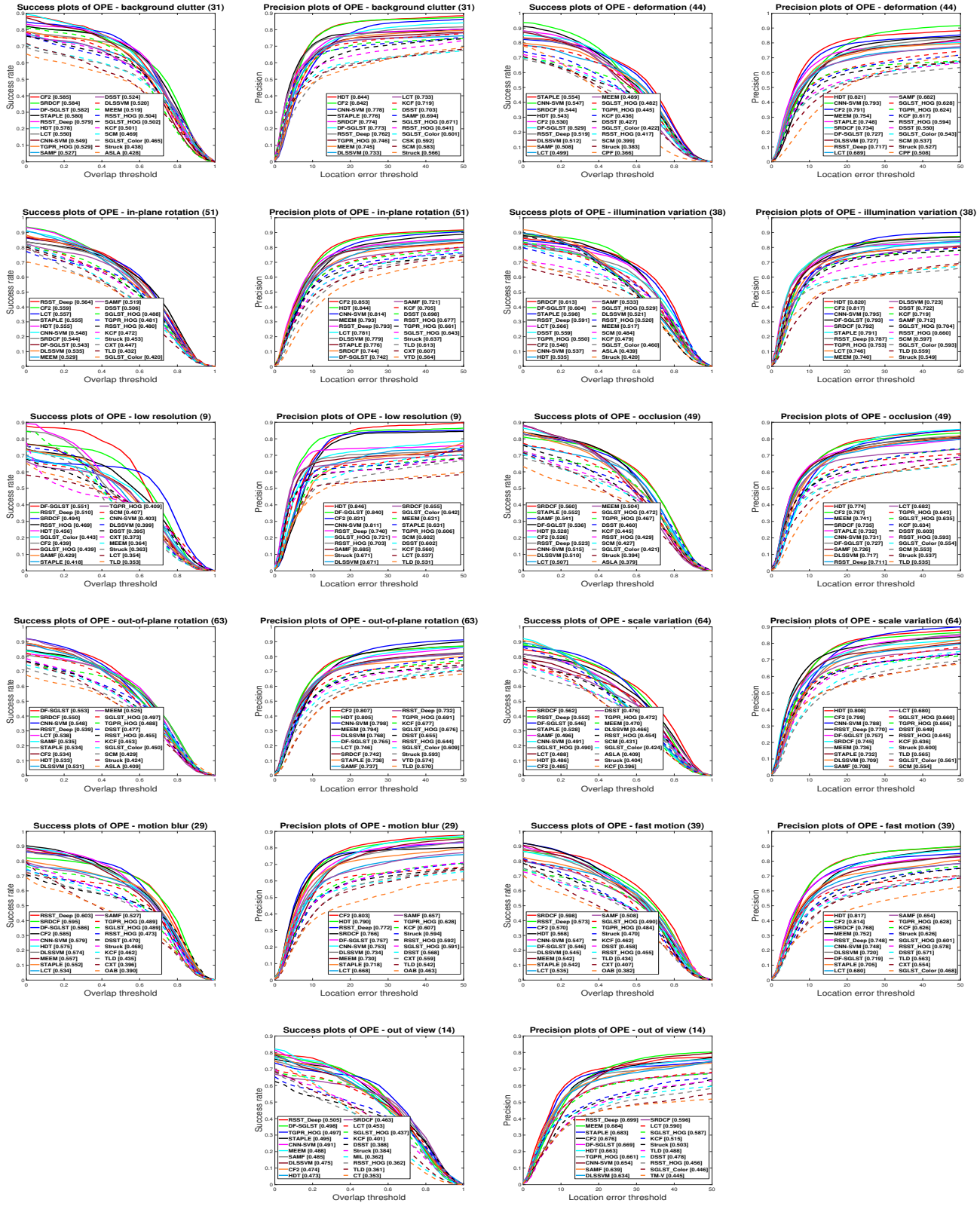

Fig. 5: The OPE success plots and precision plots for each of 11 challenge subsets in OTB100.

plates are updated with a wrong tracking result. Both lead to the error propagates throughout the sequence. In future, we will investigate an adaptive template update and particle filter resampling process to address this shortcoming and improve the performance of DF-SGLST.

6. CONCLUSIONS

In this paper, we propose a novel tracker, called deep-feature based structured group local sparse tracker (DF-SGLST), which exploits CNN deep features of local patches within target candidates in the particle filter framework. Unlike conventional local sparse trackers, DF-SGLST employs a new convex optimization model to preserve spatial layout structure among the local features. To solve the proposed optimization model, we develop an efficient numerical algorithm consisting of two subproblems with closed-form solutions based on ADMM. The extensive experimental results on OTB50 and OTB100 demonstrate that DF-SGLST outperforms various state-of-the-art methods including its two variant trackers, representative conventional and recent sparse trackers, correlation filter-based trackers, and convolutional neural network based trackers in terms of AUC and precision scores.

7. REFERENCES

[1] Alper Yilmaz, Omar Javed, and Mubarak Shah, "Object tracking: A survey," *Acm computing surveys (CSUR)*, vol. 38, no. 4, pp. 13, 2006.

[2] Samuele Salti, Andrea Cavallaro, and Luigi Di Stefano, "Adaptive appearance modeling for video tracking: Survey and evaluation," *IEEE Transactions on Image Processing*, vol. 21, no. 10, pp. 4334–4348, 2012.

[3] Yu Pang and Haibin Ling, "Finding the best from the second bests-inhibiting subjective bias in evaluation of visual tracking algorithms," in *Proceedings of the IEEE International Conference on Computer Vision*, 2013, pp. 2784–2791.

[4] Matej Kristan, Jiri Matas, Ales Leonardis, Michael Felsberg, Luka Cehovin, Gustavo Fernandez, Tomas Vojir, Gustav Hager, Georg Nebehay, and Roman Pflugfelder, "The visual object tracking vot2015 challenge results," in *Proceedings of the IEEE international conference on computer vision workshops*, 2015, pp. 1–23.

[5] Tianzhu Zhang, Si Liu, Changsheng Xu, Shuicheng Yan, Bernard Ghanem, Narendra Ahuja, and Ming-Hsuan Yang, "Structural sparse tracking," in *Proceedings of the IEEE conference on computer vision and pattern recognition*, 2015, pp. 150–158.

[6] Tianzhu Zhang, Adel Bibi, and Bernard Ghanem, "In defense of sparse tracking: Circulant sparse tracker," in *Proceedings of the IEEE conference on computer vision and pattern recognition*, 2016, pp. 3880–3888.

[7] Xue Mei and Haibin Ling, "Robust visual tracking and vehicle classification via sparse representation," *IEEE transactions on pattern analysis and machine intelligence*, vol. 33, no. 11, pp. 2259–2272, 2011.

[8] Xue Mei, Zhibin Hong, Danil Prokhorov, and Dacheng Tao, "Robust multitask multiview tracking in videos," *IEEE transactions on neural networks and learning systems*, vol. 26, no. 11, pp. 2874–2890, 2015.

[9] Xu Jia, Huchuan Lu, and Ming-Hsuan Yang, "Visual tracking via adaptive structural local sparse appearance model," in *Computer vision and pattern recognition (CVPR), 2012 IEEE Conference on*. IEEE, 2012, pp. 1822–1829.

[10] Tianzhu Zhang, Changsheng Xu, and Ming-Hsuan Yang, "Robust structural sparse tracking," *IEEE Transactions on Pattern Analysis and Machine Intelligence*, 2018.

[11] Yu-Wei Chao, Yi-Ren Yeh, Yu-Wen Chen, Yuh-Jye Lee, and Yu-Chiang Frank Wang, "Locality-constrained group sparse representation for robust face recognition," in *Image Processing (ICIP), 2011 18th IEEE International Conference on*. IEEE, 2011, pp. 761–764.

[12] Shutao Li, Haitao Yin, and Leyuan Fang, "Group-sparse representation with dictionary learning for medical image denoising and fusion," *IEEE Transactions on biomedical engineering*, vol. 59, no. 12, pp. 3450–3459, 2012.

[13] Fariba Zohrizadeh, Mohsen Kheirandishfard, and Farhad Kamangar, "Image segmentation using sparse subset selection," in *Applications of Computer Vision (WACV), 2018 IEEE Winter Conference on*. IEEE, 2018, pp. 1470–1479.

[14] Fariba Zohrizadeh, Mohsen Kheirandishfard, Kamran Ghasedidizaji, and Farhad Kamangar, "Reliability-based local features aggregation for image segmentation," in *International Symposium on Visual Computing*. Springer, 2016, pp. 193–202.

[15] Songze Tang, Nan Zhou, and Liang Xiao, "Pansharpening via locality-constrained sparse representation," in *BMVC*, 2017.

[16] Chenglong Bao, Yi Wu, Haibin Ling, and Hui Ji, "Real time robust l1 tracker using accelerated proximal gradient approach," in *Computer Vision and Pattern Recognition (CVPR), 2012 IEEE Conference on*. IEEE, 2012, pp. 1830–1837.

[17] Tianzhu Zhang, Bernard Ghanem, Si Liu, and Narendra Ahuja, "Low-rank sparse learning for robust visual tracking," in *European conference on computer vision*. Springer, 2012, pp. 470–484.

[18] Zhibin Hong, Xue Mei, Danil Prokhorov, and Dacheng Tao, "Tracking via robust multi-task multi-view joint sparse representation," in *Proceedings of the IEEE international conference on computer vision*, 2013, pp. 649–656.

[19] Baiyang Liu, Junzhou Huang, Casimir Kulikowski, and Lin Yang, "Robust visual tracking using local sparse appearance model and k-selection," *IEEE transactions on pattern analysis and machine intelligence*, vol. 35, no. 12, pp. 2968–2981, 2013.

[20] Xu Jia, Huchuan Lu, and Ming-Hsuan Yang, "Visual tracking via coarse and fine structural local sparse appearance models," *IEEE Transactions on Image processing*, vol. 25, no. 10, pp. 4555–4564, 2016.

[21] Shai Avidan, "Ensemble tracking," *IEEE transactions on pattern analysis and machine intelligence*, vol. 29, no. 2, 2007.

[22] Helmut Grabner, Christian Leistner, and Horst Bischof, "Semi-supervised on-line boosting for robust tracking," in *European conference on computer vision*. Springer, 2008, pp. 234–247.

[23] Boris Babenko, Ming-Hsuan Yang, and Serge Belongie, "Visual tracking with online multiple instance learning," in *Computer Vision and Pattern Recognition, 2009. CVPR 2009. IEEE Conference on*. IEEE, 2009, pp. 983–990.

[24] Michael J Black and Allan D Jepson, "Eigentracking: Robust matching and tracking of articulated objects using a view-based representation," *International Journal of Computer Vision*, vol. 26, no. 1, pp. 63–84, 1998.

[25] Amit Adam, Ehud Rivlin, and Ilan Shimshoni, "Robust fragments-based tracking using the integral histogram," in *Computer vision and pattern recognition, 2006 IEEE Computer Society Conference on*. IEEE, 2006, vol. 1, pp. 798–805.

[26] David A Ross, Jongwoo Lim, Ruei-Sung Lin, and Ming-Hsuan Yang, "Incremental learning for robust visual tracking," *International journal of computer vision*, vol. 77, no. 1-3, pp. 125–141, 2008.

[27] João F Henriques, Rui Caseiro, Pedro Martins, and Jorge Batista, "Exploiting the circulant structure of tracking-by-detection with kernels," in *European conference on computer vision*. Springer, 2012, pp. 702–715.

[28] João F Henriques, Rui Caseiro, Pedro Martins, and Jorge Batista, "High-speed tracking with kernelized correlation filters," *IEEE Transactions on Pattern Analysis and Machine Intelligence*, vol. 37, no. 3, pp. 583–596, 2015.

[29] Chao Ma, Jia-Bin Huang, Xiaokang Yang, and Ming-Hsuan Yang, "Hierarchical convolutional features for visual tracking," in *Proceedings of the IEEE international conference on computer vision*, 2015, pp. 3074–3082.

[30] Martin Danelljan, Gustav Häger, Fahad Khan, and Michael Felsberg, "Accurate scale estimation for robust visual tracking," in *British Machine Vision Conference, Nottingham, September 1-5, 2014*. BMVA Press, 2014.

[31] Naiyan Wang and Dit-Yan Yeung, "Learning a deep compact image representation for visual tracking," in *Advances in neural information processing systems*, 2013, pp. 809–817.

[32] Lijun Wang, Wanli Ouyang, Xiaogang Wang, and Huchuan Lu, "Visual tracking with fully convolutional networks," in *Proceedings of the IEEE international conference on computer vision*, 2015, pp. 3119–3127.

[33] Yuankai Qi, Shengping Zhang, Lei Qin, Hongxun Yao, Qingming Huang, Jongwoo Lim, and Ming-Hsuan Yang, "Hedged deep tracking," in *Proceedings of the IEEE conference on computer vision and pattern recognition*, 2016, pp. 4303–4311.

[34] Kaihua Zhang, Qingshan Liu, Yi Wu, and Ming-Hsuan Yang, "Robust visual tracking via convolutional networks without training," *IEEE Transactions on Image Processing*, vol. 25, no. 4, pp. 1779–1792, 2016.

[35] Jifeng Ning, Jimei Yang, Shaojie Jiang, Lei Zhang, and Ming-Hsuan Yang, "Object tracking via dual linear structured svm and explicit feature map," in *Proceedings of the IEEE conference on computer vision and pattern recognition*, 2016, pp. 4266–4274.

[36] Li Wang, Ting Liu, Gang Wang, Kap Luk Chan, and Qingxiong Yang, "Video tracking using learned hierarchical features," *IEEE Transactions on Image Processing*, vol. 24, no. 4, pp. 1424–1435, 2015.

[37] Hyeonseob Nam and Bohyung Han, "Learning multi-domain convolutional neural networks for visual tracking," in *Proceedings of the IEEE Conference on Computer Vision and Pattern Recognition*, 2016, pp. 4293–4302.

[38] Ilchae Jung, Jeany Son, Mooyeol Baek, and Bohyung Han, "Real-time mdnet," *arXiv preprint arXiv:1808.08834*, 2018.

[39] Stephen Boyd, Neal Parikh, Eric Chu, Borja Peleato, Jonathan Eckstein, et al., "Distributed optimization and statistical learning via the alternating direction method of multipliers," *Foundations and Trends® in Machine learning*, vol. 3, no. 1, pp. 1–122, 2011.

[40] Karen Simonyan and Andrew Zisserman, "Very deep convolutional networks for large-scale image recognition," *arXiv preprint arXiv:1409.1556*, 2014.

[41] Joseph Redmon, Santosh Divvala, Ross Girshick, and Ali Farhadi, "You only look once: Unified, real-time object detection," in *Proceedings of the IEEE conference on computer vision and pattern recognition*, 2016, pp. 779–788.

[42] Yi Wu, Jongwoo Lim, and Ming-Hsuan Yang, "Online object tracking: A benchmark," in *Proceedings of the IEEE conference on computer vision and pattern recognition*, 2013, pp. 2411–2418.

[43] Yi Wu, Jongwoo Lim, and Ming-Hsuan Yang, "Object tracking benchmark," *IEEE Transactions on Pattern Analysis and Machine Intelligence*, vol. 37, no. 9, pp. 1834–1848, 2015.

[44] Navneet Dalal and Bill Triggs, "Histograms of oriented gradients for human detection," in *Computer Vision and Pattern Recognition, 2005. CVPR 2005. IEEE Computer Society Conference on*. IEEE, 2005, vol. 1, pp. 886–893.

[45] Andrea Vedaldi and Karel Lenc, "Matconvnet: Convolutional neural networks for matlab," in *Proceedings of the 23rd ACM international conference on Multimedia*. ACM, 2015, pp. 689–692.

[46] M. Javanmardi and X. Qi, "Robust structured multi-task multi-view sparse tracking," in *2018 IEEE International Conference on Multimedia and Expo (ICME)*, July 2018, pp. 1–6.

[47] Jin Gao, Haibin Ling, Weiming Hu, and Junliang Xing, "Transfer learning based visual tracking with gaussian processes regression," in *European Conference on Computer Vision*. Springer, 2014, pp. 188–203.

[48] Dong Wang and Huchuan Lu, "Visual tracking via probability continuous outlier model," in *Proceedings of the IEEE conference on computer vision and pattern recognition*, 2014, pp. 3478–3485.

[49] Jianming Zhang, Shugao Ma, and Stan Sclaroff, "MEEM: robust tracking via multiple experts using entropy minimization," in *Proc. of the European Conference on Computer Vision (ECCV)*, 2014.

[50] Yang Li and Jianke Zhu, "A scale adaptive kernel correlation filter tracker with feature integration," in *European conference on computer vision*. Springer, 2014, pp. 254–265.

[51] Martin Danelljan, Gustav Hager, Fahad Shahbaz Khan, and Michael Felsberg, "Learning spatially regularized correlation filters for visual tracking," in *Proceedings of the IEEE International Conference on Computer Vision*, 2015, pp. 4310–4318.

[52] Luca Bertinetto, Jack Valmadre, Stuart Golodetz, Ondrej Miksik, and Philip HS Torr, "Staple: Complementary learners for real-time tracking," in *Proceedings of the IEEE conference on computer vision and pattern recognition*, 2016, pp. 1401–1409.

[53] Wei Zhong, Huchuan Lu, and Ming-Hsuan Yang, "Robust object tracking via sparsity-based collaborative model," in *Computer vision and pattern recognition (CVPR), 2012 IEEE Conference on*. IEEE, 2012, pp. 1838–1845.

[54] Sam Hare, Stuart Golodetz, Amir Saffari, Vibhav Vineet, Ming-Ming Cheng, Stephen L Hicks, and Philip HS Torr, "Struck: Structured output tracking with kernels," *IEEE transactions on pattern analysis and machine intelligence*, vol. 38, no. 10, pp. 2096–2109, 2016.

[55] Tianzhu Zhang, Bernard Ghanem, Si Liu, and Narendra Ahuja, "Robust visual tracking via multi-task sparse learning," in *Computer vision and pattern recognition (CVPR), 2012 IEEE conference on*. IEEE, 2012, pp. 2042–2049.

[56] Chao Ma, Xiaokang Yang, Chongyang Zhang, and Ming-Hsuan Yang, "Long-term correlation tracking," in *Proceedings of the IEEE conference on computer vision and pattern recognition*, 2015, pp. 5388–5396.

[57] Jongwon Choi, Hyung Jin Chang, Sangdoo Yun, Tobias Fischer, Yiannis Demiris, Jin Young Choi, et al., "Attentional correlation filter network for adaptive visual tracking.," in *CVPR*, 2017, vol. 2, p. 7.

[58] David Held, Sebastian Thrun, and Silvio Savarese, "Learning to track at 100 fps with deep regression networks," in *European Conference on Computer Vision*. Springer, 2016, pp. 749–765.

[59] Seunghoon Hong, Tackgeun You, Suha Kwak, and Bohyung Han, "Online tracking by learning discriminative saliency map with convolutional neural network," in *International Conference on Machine Learning*, 2015, pp. 597–606.

[60] Luca Bertinetto, Jack Valmadre, Joao F Henriques, Andrea Vedaldi, and Philip HS Torr, "Fully-convolutional

siamese networks for object tracking," in *European conference on computer vision*. Springer, 2016, pp. 850–865.